Harnessing Viscoelasticity to Suppress Irreversibility Buildup in a Colloidal Stirling Engine

Niloyendu Roy,[1] A. K. Sood,[2,3] and Rajesh Ganapathy[3,4]
[1]*Chemistry and Physics of Materials Unit, Jawaharlal Nehru Centre for Advanced Scientific Research, Jakkur, Bangalore—560064, India*
[2]*Department of Physics, Indian Institute of Science, Bangalore—560012, India*
[3]*International Centre for Materials Science, Jawaharlal Nehru Centre for Advanced Scientific Research, Jakkur, Bangalore—560064, India*
[4]*School of Advanced Materials (SAMat), Jawaharlal Nehru Centre for Advanced Scientific Research, Jakkur, Bangalore—560064, India*

(Received 18 May 2023; revised 18 July 2023; accepted 8 November 2023; published 7 December 2023)

Typically, the rate at which a heat engine can produce useful work is constrained by the buildup of irreversibility with increasing operating speed. Here, using a recently developed reservoir engineering technique, we designed and quantified the performance of a colloidal Stirling engine operating in a viscoelastic bath. While the bath acts like a viscous fluid in the quasistatic limit, and the engine's performance agrees with equilibrium predictions, on reducing the cycle time to the bath's structural relaxation time, the increasingly elastic response of the bath aids suppress the buildup of irreversibility. We show that the elastic energy stored during the isothermal compression step of the Stirling cycle facilitates quick equilibration in the isothermal expansion step. This results in equilibriumlike efficiencies even for cycle times shorter than the equilibration time of the colloidal particle.

DOI: 10.1103/PhysRevLett.131.238201

Mesoscale heat engines, wherein a single atom [1] or a colloidal particle [2–9] is typically the working substance, are proving to be indispensable in understanding heat-to-work conversion in a fluctuation-dominated regime. The early experimental realization of these engines executed standard thermodynamic cycles and found that their cycle-averaged performance mirrored their macroscopic siblings [10], as predicted [11–14]. More recently, experiments with colloidal heat engines have enabled probing the mechanism (s) of energy transfer in a regime with no obvious macroscale counterpart. These include engines operating between reservoirs with nonthermal noise statistics [15], like those containing live bacteria [4], or engineered non-Gaussian baths with δ-correlated noise [5]. While bacterial baths have been proven to enhance the quasistatic performance, non-Gaussian baths have been found to influence the nature of irreversibility and the statistics of the stochastic energetics of engines. Although these studies have nicely demonstrated that altering the nature of noise statistics allows tuning the performance of mesoscale engines, in all prior studies, the bath itself was purely dissipative with a clear separation of timescales between the relaxation of the bath fluid and the colloidal working substance. In contrast, in structured fluids, like gels, the relaxation times are often large, and dissipation experienced by the colloid in such baths has a memory dependence [16], which influences their response, especially when driven out of equilibrium [17–20]. Thus, even naively, we expect the frequency-dependent viscoelastic properties of a structured bath to feed into mesoscale engines' performance for finite-duration thermodynamic cycles. While in any engine, be it macro- or mesoscale, irreversibility creeps in for finite-duration cycles due to the inability of the working substance to equilibrate, which limits the window of cycle times over which useful work is extracted [2,5,10], a recent numerical study [21] anticipates a broader window for a Stirling cycle performed in a viscoelastic bath instead of a viscous one with the same zero-shear viscosity. Although non-Newtonian fluids are more ubiquitous than Newtonian fluids and examples from biology abound, consider a molecular motor carrying cargo inside a living cell—a viscoelastic broth [22]; there is as yet no experimental realization of a mesoscale heat engine operating in a viscoelastic environment.

Here, we build and quantify the performance of a colloidal Stirling engine operating in a viscoelastic bath. Central to our experiments is a reservoir engineering approach [5] that allowed us to execute thermodynamic cycles without physically heating or cooling the gel. However, unlike in [5] where a non-Gaussian noise was imposed on the colloidal particle in a viscous medium, here the imposed noise is Gaussian. We exploit this ability to disentangle the role of viscoelasticity on engine performance. A key finding of our Letter is we show directly that the elasticity of the gel aids suppress the buildup of irreversibility as the Stirling cycle duration approaches the gels' relaxation time from above and results in a near quasistaticlike performance of the engine.

Our mesoscale Stirling engine comprised of an optically trapped polystyrene colloid (diameter $\sigma = 1.37$ μm, Bangs Labs USA)—the working substance—that is suspended in a surfactant gel—a canonical viscoelastic bath [see Supplemental Material (S1)]. Above the Krafft temperature of 296 K, the gel is an entangled network of cylindrical wormlike micelles [23,24]. We observed that the position (see Supplemental Material S3, [25,26] for acquisition methods) fluctuations of the trapped colloid were Gaussian (see Fig. S1 and Supplemental Material S2), allowing us to determine the trap stiffness k_1 from the energy equipartition relation, $k_1 \langle x^2 \rangle /2 = k_B T/2$. Here, k_B is the Boltzmann constant, and T is the bath temperature. Executing a *standard* thermodynamic cycle, like the Stirling cycle, with the trapped colloid requires periodically varying k_1 and T. Modulating T via the physical heating and cooling of the viscoelastic gel, however, can fundamentally alter its phase behavior and rheology. Furthermore, for thermodynamic cycles of finite duration—a regime of practical importance—quantifying how the gel rheology is modified by rapid temperature changes is challenging. We sidestepped this difficulty by leaning on a technique [5] (see Supplemental Material S4) developed by us earlier, wherein a trapped colloid's effective temperature can be manipulated by imposing an additional noise on the colloid from a second flashing optical trap. This is achieved via an independent holographic optical trap that is coupled to the same imaging objective (Leica Plan Apochromat 100x, N.A. 1.4, oil) as the primary trap. This second trap with stiffness k_2 is flashed at a frequency of 34 Hz at different distances $\delta a(t)$ along the x axis [see Fig. 1(a)]. The distribution of $\delta a(t)$, in the present study, is a Gaussian [Fig. 1(b)] that is peaked at the center of the primary trap, and the effective stiffness is $k = k_1 + k_2$ [5,27,28]. In Fig. 1(c), we compare the particle's position probability distribution $\rho(x)$, when the second optical trap is flashed (red circles), with when it is stationary and centered on the primary trap (black squares). Applying equipartition yields an effective temperature T_{eff} of 452 K when the trap is flashed and 298 K when it is not. Because the tweezer does not couple to the background gel medium, this approach enables the implementation of thermodynamic cycles without altering the gel rheology. Our approach is, thus, advantageous over electrophoretic noise techniques [29] where the noisy electric field can couple directly to the positively charged wormlike micelles.

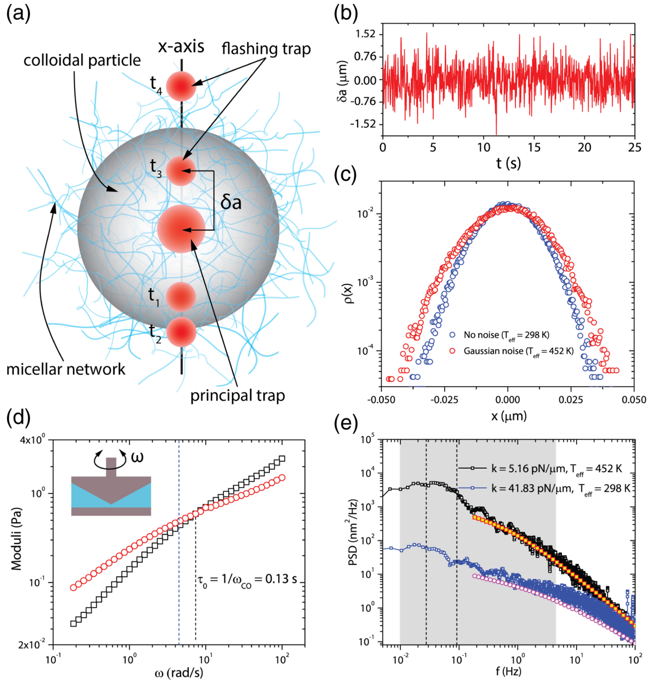

FIG. 1. (a) The primary trap is represented by the big red spot. The secondary trap at different time instances, t_1, t_2, t_3, and t_4 is represented by the small red spots. (b) Gaussian distributed $\delta a(t)$ that results in a $\rho(x)$ represented by the red circles in (c), corresponding to $T_{\mathrm{eff}} = 452$ K. Blue circles in (c) correspond to $T_{\mathrm{eff}} = 298$ K when $\delta a(t) = 0$ at all times. The trapping stiffness was fixed at $k = 41.83$ pN/μm. (d) Black squares (red circles) represent bulk G' (G'') as a function of ω in the gel rheology with cone-plate geometry (schematic at top left). Black dotted line indicates the crossover of G' and G'' at ω_{CO}. Blue dotted line indicates the minimum duration $\tau = 0.5$ of the Stirling cycles performed. (e) For $k = 5.16$ pN/μm (41.83 pN/μm) and $T_{\mathrm{eff}} = 452$ K (298 K), PSD directly calculated from the particle's position, x and $\mathrm{PSD}_{\mathrm{FDT}}$ calculated from bulk G' and G'' are shown by black (blue) squares and magenta circles (yellow squares), respectively. Gray shaded region indicates the range of τ. Black dotted lines mark the region where PSDs saturate.

Before a Stirling engine can be constructed, yet another aspect associated with the structured nature of the bath fluid needs to be addressed. For a Stirling engine operating in a viscoelastic bath in the quasistatic limit, i.e., the cycle time $\tau \to \infty$, the Deborah number De, defined by the ratio of the timescale of the material's relaxation to the timescale of observation, is much less than 1, and the bath's response will be typical of a viscous fluid [16]. For finite τ, however, both viscous and elastic responses will contribute to varying extents depending on how τ compares with the structural relaxation τ_0 of the gel. We determined τ_0 from a standard frequency-sweep measurement done on a commercial rheometer (see Supplemental Material S5 and Fig. S2) using a cone-plate geometry [Fig. 1(d)]. The frequency (ω) dependence of the bulk elastic and viscous moduli, $G'(\omega)$ and $G''(\omega)$, respectively, was typical of semidilute wormlike micellar gels, with the crossover frequency ω_{CO} of G' and G'' yielding $\tau_0 = 1/\omega_{\mathrm{CO}} = 0.13$ s (dashed black vertical line). However, before we can rely on these measurements to guide the operation of our Stirling engine, it is essential to determine if the microrheological gel response sampled by the trapped colloid agrees with the macrorheological one. We quantified the microrheological response of the gel via the power spectral density (PSD) of the trapped particle's position for two different values of k and $T_{\rm eff}$ [Fig. 1(e)]. Here, black squares correspond to $k = 5.2$ pN/μm and $T_{\rm eff} = 452$ K, and blue squares to $k = 41.9$ pN/μm and $T_{\rm eff} = 298$ K. If micro- and macrorheology agree, then the experimentally obtained PSD must fit

$$\mathrm{PSD}_{\rm FDT}(f) = \frac{2k_BT}{\pi f}\frac{6\pi\sigma G''(f)}{[k + 6\pi\sigma G'(f)]^2 + [6\pi\sigma G''(f)]^2} \qquad (1)$$

obtained from the generalized fluctuation-dissipation theorem [17,20]. We computed $\mathrm{PSD}_{\rm FDT}$ by plugging in the appropriate k and $T_{\rm eff}$ and the G' and G'' obtained from bulk rheology [filled symbols in Fig. 1(e)]. The agreement between micro- and macrorheology is rather good [30]. This observation is consistent with the fact that the particle is much larger than the mesh size (≈100 nm) [31] of the gel network and hence samples the long-wavelength rheological properties. Moreover, for the same k values, the PSDs in the engineered bath at $T_{\rm eff} = 452$ K are shifted parallel (Supplemental Material S6, Fig. S3) with respect to the PSDs at $T_{\rm eff} = 298$ K for $f \leq 20$ Hz, implying that the flashing trap noise indeed acts like an effective temperature in the regime of interest.

Banking on our ability to tune $T_{\rm eff}$ without altering the gel rheology, we designed a Stirling engine operating between a hot reservoir at temperature $T^H_{\rm eff} = 452$ K and a cold reservoir at $T^C_{\rm eff} = 298$ K. The Stirling cycle comprised of an isothermal compression (path ①–②) and expansion step (path ③–④) linked by two isochoric transitions (paths ②–③ and ④–①) [see Fig. 2(a), Supplemental Material S8, and Fig. S5]. While the isothermal processes involved a linear modulation of the effective stiffness between $5.16\ \mathrm{pN/μm} \leq k \leq 41.83\ \mathrm{pN/μm}$, the isochoric transitions were carried out by switching "on" (path ②–③) or "off" (path ④–①) the flashing trap noise. The widths of the equilibrium $\rho(x)$ measured at the four state points are clearly reflective of the standard Stirling protocol (Supplemental Material S8 and Fig. S5). We continuously executed many hundreds of Stirling cycles for each cycle duration, and these spanned more than two decades $0.5\ \mathrm{s} < \tau < 200\ \mathrm{s}$. The lower limit of τ, which is comparable to τ_0, was chosen to be at least a decade larger than the flashing noise frequency to ensure proper sampling of the external noise by the particle. To further ensure that the external noise in our protocol is capable of engineering baths that are at equilibrium and at an effective temperature, we compared the operation of the Stirling engine in the viscoelastic medium with a Stirling engine operated in a viscous medium (Supplemental Material S7, Fig. S4) where the bath temperatures are engineered using an identical protocol as described in Fig. 1(a).

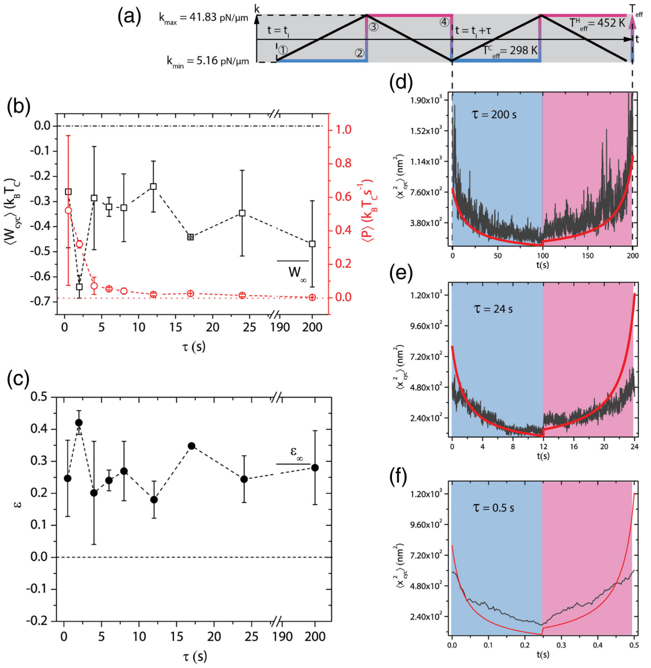

FIG. 2. (a) Protocol for k and $T_{\rm eff}$ modulation with respect to time for executing the Stirling cycles with equilibrium state points ① → ④. (b) $\langle W_{\rm cyc}\rangle$ (black squares) and $\langle P\rangle$ (red circles) as a function of τ. The black (red) dotted line corresponds to zero work (power) output. (c) The efficiency ε as a function of τ. $\varepsilon = 0$ is marked with a black dotted line. In (b) and (c), the black solid line segments indicate the Stirling saturation work (W_∞) and efficiency (ε_∞), respectively. The error bars represent the standard deviation in the mean quantities across different experiments (Supplemental Material S8). The dark gray curves in (d), (e) and (f) show $\langle x^2_{\rm cyc}\rangle$ as a function of time for $\tau = 200$ s, $\tau = 24$ s and $\tau = 0.5$ s, respectively. The cold (hot) isotherm is shaded blue (red). The red curve in (d), (e) and (f) represents theoretically calculated $k_BT_{\rm eff}/k$.

Following standard procedures [32–34], we quantified the performance of our Stirling engine. The work done per cycle, $W_{\rm cyc}$, is the change in the potential energy, U, of the particle due to the modulation of the primary trap stiffness: $W_{\rm cyc} = \int_{t_i}^{t_i+\tau}(\partial U/\partial k)\circ dk \equiv \frac{1}{2}\int_{t_i}^{t_i+\tau} x^2\circ dk$. Here, t_i denotes the start of the ith cycle, and $\circ$ represents a Stratonovich product. The efficiency, $\varepsilon = (W_{\rm cyc}/\langle Q_h\rangle)$, where $\langle Q_h\rangle$ is the sum of the heat $Q_{2\to3}$ absorbed during the isochoric heating, and the heat $Q_{3\to4}$ exchanged during the isothermal expansion steps (Supplemental Material S9), and $\langle\rangle$ denotes an averaging over cycles. In Figs. 2(b) and 2(c), we plot $\langle W_{\rm cyc}\rangle$ (black squares) and $\langle\varepsilon\rangle$ for various values of τ, respectively. For the longest cycle duration ($\tau = 200\ \mathrm{s} \gg \tau_0$), $\langle W_{\rm cyc}\rangle$ and $\langle\varepsilon\rangle$ agree well with the theoretically predicted Stirling saturation work, $W_\infty = k_B(T^C_{\rm eff} - T^H_{\rm eff})\ln\sqrt{k_{\rm max}/k_{\rm min}}$ [horizontal bar in Fig. 2(a)] and the equilibrium Stirling efficiency, $\varepsilon_\infty = \varepsilon_C(1 + \varepsilon_C/\ln(k_{\rm max}/k_{\rm min}))^{-1}$ [horizontal bar in Fig. 2(b)], respectively.

Here, $\varepsilon_C = 1 - (T^C_{\mathrm{eff}}/T^H_{\mathrm{eff}})$ is the Carnot efficiency. The engine operated in the quasistatic limit, as expected [21]. On reducing τ, however, $\langle W_{\mathrm{cyc}} \rangle$ and $\langle \varepsilon \rangle$ continue to hover near W_∞ and ε_∞, respectively, and the average power $\langle P \rangle = \langle W_{\mathrm{cyc}} \rangle / \tau$ (red circles) increases monotonically. This observation implies that the particle continues to explore a substantial fraction of the available phase volume on lowering τ. To strengthen this inference, we calculated the mean-squared position $\langle x^2_{\mathrm{cyc}} \rangle$ of the particle at different instances of a cycle for $\tau = 200$ s, $\tau = 24$ s, and $\tau = 0.5$ s, respectively [Figs. 2(d)–2(f)]. Here, the $\langle \rangle$ brackets denote averaging over time instances separated by τ. For all values of τ, the isothermal compression, the isochoric heating, and the isothermal expansion [Fig. 2(a)] is manifest clearly as a gradual decrease, short step increase, and a gradual increase of $\langle x^2_{\mathrm{cyc}} \rangle$. While for $\tau = 200$ s, the values of $\langle x^2_{\mathrm{cyc}} \rangle$ at different state points agree with equilibrium values [red curve in Fig. 2(d)], for $\tau = 24$ s, and especially, $\tau = 0.5$ s, which is far from the quasistatic limit, the exploration of the volume is still substantial, which, combined with the fact that ε and $\langle W_{\mathrm{cyc}} \rangle$ are nearly flat, points toward the suppression of irreversibility in the engine.

The small τ behavior of our Stirling engine is quite intriguing, when placed in the context of the equilibrium PSD shown in Fig. 1(e). Here we see a roll off at $f_c \sim 0.1$ Hz and a plateau for $f < f_c$ for $T_{\mathrm{eff}} = 452$ K. Thus, an isothermal expansion step with a duration $(\tau/2) > (1/f_c) \sim 10$ s lies in the plateau portion of the PSD, and the particle has time to explore if not fully, to a considerable extent, the available phase volume. Thus the work that the particle performs is comparable to W_∞, and the observed modulation in $\langle x^2_{\mathrm{cyc}} \rangle$ is expected. However, for the smallest τ studied here, the PSD at the corresponding frequency has fallen by nearly 2 orders of magnitude. Thus, the particle can typically explore only a tenth of the available volume during a Stirling cycle and this should result in substantial irreversibility and stalling of the engine. A quasistatic-like performance at these τ values is completely unexpected. In fact, in a viscous bath, the particle hardly explores the volume ($\langle x^2_{\mathrm{cyc}} \rangle$ is small and constant) when the trap stiffness is modulated at a frequency where the PSD is one-hundredth of the corresponding plateau value (Supplemental Material S10, S11, and Fig. S6, S7).

The answer to how a viscoelastic bath aids in suppresssinig the buildup of irreversibility in the engine at small τ has to lie in dynamics of volume exploration by the particle. In Fig. 3(a), we show the mean-squared displacement (MSD_x) of the particle during engine operation for various τ. For all τ, the MSD_x plateaus at long times to roughly the same value, i.e., when the particle reaches the walls of the confining potential. The ripples observed here have a period of τ and are simply due to the cyclic operation of the engine. The short-time behavior of the MSD_x, however, is quite revealing. For large τ, the particle dynamics is subdiffusive, $\mathrm{MSD}_x \propto t^\alpha$ with $\alpha \approx 0.5$ for $\tau = 200$ s, due to the structured nature of the bath [35]. Remarkably, as τ is lowered, α increases, implying a faster exploration of the volume by the particle. We compared this finding with a viscous bath (Supplemental Material S12 and Fig. S8) where we observed that at short times the MSD_x is diffusive ($\alpha = 1$) irrespective of τ and also the plateau occurred at smaller values on decreasing τ consistent with poor volume exploration.

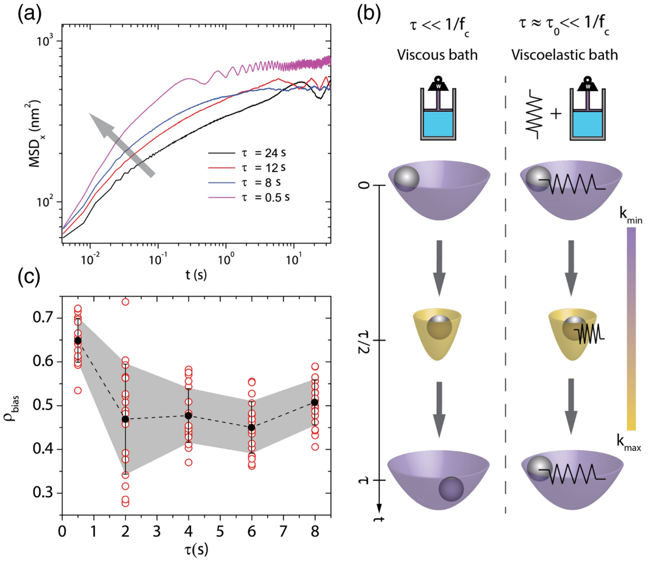

FIG. 3. (a) MSD_x as a function of time, t, for $\tau = 24$ s (black line), $\tau = 12$ s (red line), $\tau = 8$ s (blue line), and $\tau = 0.5$ s (magenta line). The gray arrow indicates the increase in the slope of MSD_x with decreasing τ. (b) Schematic diagram of the role of elasticity in volume exploration. Here the paraboloids represent the breathing potential at different states and are color coded according to the corresponding k values. (c) ρ_{bias} calculated over 100 randomly picked cycles (Supplemental Material S13) as a function of τ. Red circles represent each random picking. The corresponding mean values are shown by the black circles. The shaded region indicates the standard deviation from the mean.

As τ approaches τ_0, G' begins to play an increasing role [Fig. 1(d)] and the faster volume exploration at these τ should have its origins in the gel elasticity. Figure 3(b) schematically captures the mechanism possibly at play. Let us consider a cycle that begins with the particle residing at an extreme of the confining potential (top panel). The isothermal compression step (① → ②) over an interval of $\tau/2$, drives the particle toward the center and compresses the gel network. If $\tau/2 \approx \tau_0$, the gel is unable to relax and the stored elastic energy from the compression aids the particle to rapidly climb up the potential during the isothermal expansion step (③ → ④). This mechanism is consistent with the rapid equilibration seen in Fig. 3(a) when $\tau \approx \tau_0$. The gel elasticity-mediated volume exploration, however, introduces a directionality, i.e., at the end of the engine cycle, the particle is more likely to end up in the vicinity of where it was at the start of the cycle. This is quite unlike in a viscous bath where the exploration of the volume in the isothermal expansion step is purely diffusive and hence nondirectional [2,5].

To demonstrate that signatures of directional volume equilibration grow when τ approaches τ_0, we considered cycles wherein the particle at the beginning of the cycle is located far away from the trap center so that the gel network is substantially deformed during the compression step. We chose this threshold distance to be $|x(t_i)| > 20$ nm, which corresponds to two-thirds of the maximum displacement observed at state point ① (see Supplemental Material S8, S13, and Fig. S5). We then calculated the probability, ρ_{bias}, that on completion of the cycle, the particle ends up on the same side of the origin as it started from (see Supplemental Material S13). When the gel structure is able to relax during the isothermal compression step, volume equilibration in the expansion step is purely via diffusion and ρ_{bias} should hover around 0.5. This is indeed the case for $\tau > 2$ s [Fig. 3(c)]. However for $\tau = 0.5$ s, i.e., when $G' \approx G''$ [see Fig. 1(d)], $\rho_{\mathrm{bias}} \approx 0.65$ a clear sign of elasticity-mediated directional volume equilibration. As a check, when we considered cycles where the particle at the start of the cycle is located below the threshold value (see Fig. S9 and Supplemental Material S14) so that the deformation of the gel network during the compression step is small, $\rho_{\mathrm{bias}} \approx 0.5$ for all τ.

To summarize, by exploiting a recently developed reservoir engineering approach [5], we have uncovered how the viscoelasticity of the bath feeds into the performance of a Stirling engine. In the quasistatic limit, the bath acts like a purely viscous fluid, and our Stirling engine's experimentally determined work and efficiency agree with equilibrium predictions. On lowering the cycle time toward the bath's relaxation time, the increasing elastic contribution of the gel microstructure aids rapid volume exploration of the colloid and suppresses the buildup of irreversibility. Remarkably, thus, our engine delivers a quasistatic-like performance even when the cycle times are smaller than the equilibration time of the colloidal particle. While our apparatus precludes access to cycle times in the gel's elasticity-dominated regime, we note that here, the particle will remain strongly caged during all parts of the Stirling cycle, and we expect little or no useful work out of the engine. Therefore, cycle durations near the structured bath's relaxation time are optimal for extracting maximum power from a mesoscale engine. While our Letter is the first attempt to experimentally investigate the role of long-wavelength viscoelasticity in the functioning of a mesoscale engine, a natural step forward would be to design engines where the size of the working substance is comparable to the mesh size of the viscoelastic network. In such engines, the viscoelastic response itself depends on the size of the working substance [36] and can thus offer insights into the functioning of general fluctuation-based motors.

N. R. thanks Jawaharlal Nehru Centre for Advanced Scientific Research, Bangalore, for financial support from a student fellowship. A. K. S. thanks the Science and Engineering Board (SERB), GoI, for a support under the National Science Chair Professorship. R. G. thanks Jawaharlal Nehru Centre for Advanced Scientific Research, Bangalore, for financial support.

[1] J. Roßnagel, S. T. Dawkins, K. N. Tolazzi, O. Abah, E. Lutz, F. Schmidt-Kaler, and K. Singer, A single-atom heat engine, Science **352**, 325 (2016).
[2] V. Blickle and C. Bechinger, Realization of a micrometre-sized stochastic heat engine, Nat. Phys. **8**, 143 (2012).
[3] I. A. Martínez, É. Roldán, L. Dinis, D. Petrov, J. M. Parrondo, and R. A. Rica, Brownian carnot engine, Nat. Phys. **12**, 67 (2016).
[4] S. Krishnamurthy, S. Ghosh, D. Chatterji, R. Ganapathy, and A. Sood, A micrometre-sized heat engine operating between bacterial reservoirs, Nat. Phys. **12**, 1134 (2016).
[5] N. Roy, N. Leroux, A. Sood, and R. Ganapathy, Tuning the performance of a micrometer-sized stirling engine through reservoir engineering, Nat. Commun. **12**, 4927 (2021).
[6] S. Krishnamurthy, R. Ganapathy, and A. Sood, Synergistic action in colloidal heat engines coupled by non-conservative flows, Soft Matter **18**, 7621 (2022).
[7] P. A. Quinto-Su, A microscopic steam engine implemented in an optical tweezer, Nat. Commun. **5**, 5889 (2014).
[8] S. Ciliberto, Experiments in stochastic thermodynamics: Short history and perspectives, Phys. Rev. X **7**, 021051 (2017).
[9] I. A. Martínez, É. Roldán, L. Dinis, and R. A. Rica, Colloidal heat engines: A review, Soft Matter **13**, 22 (2017).
[10] F. L. Curzon and B. Ahlborn, Efficiency of a carnot engine at maximum power output, Am. J. Phys. **43**, 22 (1975).
[11] T. Schmiedl and U. Seifert, Efficiency at maximum power: An analytically solvable model for stochastic heat engines, Europhys. Lett. **81**, 20003 (2007).
[12] M. Esposito, R. Kawai, K. Lindenberg, and C. Van den Broeck, Efficiency at maximum power of low-dissipation carnot engines, Phys. Rev. Lett. **105**, 150603 (2010).
[13] G. Verley, M. Esposito, T. Willaert, and C. Van den Broeck, The unlikely Carnot efficiency, Nat. Commun. **5**, 4721 (2014).
[14] S. Rana, P. Pal, A. Saha, and A. Jayannavar, Single-particle stochastic heat engine, Phys. Rev. E **90**, 042146 (2014).
[15] R. Zakine, A. Solon, T. Gingrich, and F. Van Wijland, Stochastic stirling engine operating in contact with active baths, Entropy **19**, 193 (2017).
[16] R. G. Larson, *The Structure and Rheology of Complex Fluids* (Oxford University Press, New York, 1999), Vol. 150.
[17] D. Mizuno, D. Head, F. MacKintosh, and C. Schmidt, Active and passive microrheology in equilibrium and non-equilibrium systems, Macromolecules **41**, 7194 (2008).
[18] J. Berner, B. Müller, J. R. Gomez-Solano, M. Krüger, and C. Bechinger, Oscillating modes of driven colloids in over-damped systems, Nat. Commun. **9**, 999 (2018).

[19] S. Toyabe and M. Sano, Energy dissipation of a Brownian particle in a viscoelastic fluid, Phys. Rev. E **77**, 041403 (2008).

[20] J. R. Gomez-Solano and C. Bechinger, Probing linear and nonlinear microrheology of viscoelastic fluids, Europhys. Lett. **108**, 54008 (2014).

[21] J. R. Gomez-Solano, Work extraction and performance of colloidal heat engines in viscoelastic baths, Front. Phys. **9**, 643333 (2021).

[22] M. Guo, A. J. Ehrlicher, M. H. Jensen, M. Renz, J. R. Moore, R. D. Goldman, J. Lippincott-Schwartz, F. C. Mackintosh, and D. A. Weitz, Probing the stochastic, motor-driven properties of the cytoplasm using force spectrum microscopy, Cell **158**, 822 (2014).

[23] J. Soltero, J. Puig, O. Manero, and P. Schulz, Rheology of cetyltrimethylammonium tosylate-water system. 1. Relation to phase behavior, Langmuir **11**, 3337 (1995).

[24] M. Cates and S. Candau, Statics and dynamics of worm-like surfactant micelles, J. Phys. Condens. Matter **2**, 6869 (1990).

[25] See Supplemental Material, which includes Ref. [26], at http://link.aps.org/supplemental/10.1103/PhysRevLett.131.238201 for acquisition methods.

[26] R. Parthasarathy, Rapid, accurate particle tracking by calculation of radial symmetry centers, Nat. Methods **9**, 643333 (2021).

[27] A. Bérut, A. Petrosyan, and S. Ciliberto, Energy flow between two hydrodynamically coupled particles kept at different effective temperatures, Europhys. Lett. **107**, 60004 (2014).

[28] M. Chupeau, B. Besga, D. Guéry-Odelin, E. Trizac, A. Petrosyan, and S. Ciliberto, Thermal bath engineering for swift equilibration, Phys. Rev. E **98**, 010104(R) (2018).

[29] I. A. Martinez, E. Roldán, J. M. Parrondo, and D. Petrov, Effective heating to several thousand kelvins of an optically trapped sphere in a liquid, Phys. Rev. E **87**, 032159 (2013).

[30] F. Scheffold, S. Romer, F. Cardinaux, H. Bissig, A. Stradner, L. Rojas-Ochoa, V. Trappe, C. Urban, S. Skipetrov, L. Cipelletti *et al.*, New trends in optical microrheology of complex fluids and gels, *Trends in Colloid and Interface Science XVI* (Springer, Berlin, Heidelberg, 2004), pp. 141–146, 10.1007/978-3-540-36462-7_32.

[31] J. Soltero, J. Puig, and O. Manero, Rheology of the cetyltrimethylammonium tosilate-water system. 2. Linear viscoelastic regime, Langmuir **12**, 2654 (1996).

[32] K. Sekimoto, Langevin equation and thermodynamics, Prog. Theor. Phys. Suppl. **130**, 17 (1998).

[33] K. Sekimoto, *Stochastic Energetics* (Springer, New York, 2010), Vol. 799.

[34] U. Seifert, Stochastic thermodynamics, fluctuation theorems and molecular machines, Rep. Prog. Phys. **75**, 126001 (2012).

[35] I. Wong, M. Gardel, D. Reichman, E. R. Weeks, M. Valentine, A. Bausch, and D. A. Weitz, Anomalous diffusion probes microstructure dynamics of entangled f-actin networks, Phys. Rev. Lett. **92**, 178101 (2004).

[36] J. Liu, L Gardel, K. Kroy, E. Frey, B. D. Hoffman, J. C. Crocker, A. R. Bausch, and D. A. Weitz, Microrheology probes length scale dependent rheology, Phys. Rev. Lett. **96**, 118104 (2006).